PHYSICAL REVIEW B **79**, 060407(R) (2009)

Antivortex domain walls observed in permalloy rings via magnetic force microscopy

P. E. Roy,* J. H. Lee, T. Trypiniotis, D. Anderson, G. A. C. Jones, D. Tse, and C. H. W. Barnes
Cavendish Laboratory, University of Cambridge, Cambridge CB3 0HE, United Kingdom

(Received 26 November 2008; revised manuscript received 21 January 2009; published 18 February 2009)

Magnetic domain walls in patterned permalloy ring elements of different widths and thicknesses have been probed by magnetic force microscopy and micromagnetic simulations. We report the experimental observation of antivortex structures in single-layer magnetic rings, previously only theoretically predicted. Furthermore, vortex-antivortex chains are observed on occasion in wider rings that prefer a circulating flux closure state. It is possible that they are pinned transient states of the relaxation path from the magnetically saturated to the circulating flux closure state. Similar tendencies are seen in micromagnetic simulations implying that vortex-antivortex pair nucleation and annihilation are fundamental parts of the said relaxation. Finally we present a phase diagram of different domain-wall configurations as a function of ring width and thickness.

DOI: 10.1103/PhysRevB.79.060407 PACS number(s): 75.60.Ch, 75.75.+a

Microscopic ferromagnetic rings have attracted a broad interest and are currently the subject of intense research because they can easily be switched between different domain configurations with in-plane magnetic fields.[1–5] Furthermore, the possible magnetic domain configurations can be controlled by varying the ring dimensions. Different types of magnetic domain walls are known to exist in thin-film rings and strips: the transverse (symmetric and asymmetric) and vortex types.[6–10] Within the class of vortex types, the most commonly reported one in rings is the single-vortex (V^+) wall structure. In rings, domain walls occur in pairs, constituting what is known as the onion state.[11] The onion state is typically nucleated upon application and removal of a saturating in-plane magnetic field. In addition, there is the circulating flux (CF) closure state whereby the magnetization curves along the entire perimeter of the ring.[12] Recently, the two-vortex ($2V^+$) wall structure, which occurs in thicker and wider rings, was observed by magnetic force microscopy (MFM).[13] Micromagnetic simulations by Park *et al.*[13] also suggest that walls having both V^+ and antivortex (V^-) structures (Fig. 1)[14,15] may exist in rings but these were not observed experimentally. Similar predictions for magnetic strips have been made by McMichael and Donahue.[6] Klaui *et al.*[16] reported on the transformation of V^+ to $2V^+$ wall structures with a V^- structure in between in NiFe wires upon injecting a spin-current. It was recently found by micromagnetic simulations that formation and annihilation of V^+V^- pairs is a fundamental process in nanoscale magnetization dynamics and that the annihilation can cause burstlike dissipation of exchange energy released as spin waves.[17–19] Such processes were proposed as the basis for spin-wave radiators in future logic devices.[20] Experimentally, the dynamical properties of a V^- trapped in between two V^+ structures in a permalloy platelet were measured by Kuepper *et al.*[21]

We report herein the experimental finding of V^- structures at remanence in single-layer magnetic rings, in particular the $V^+V^-V^+$ configuration, i.e., two V^+ structures with a V^- in between (Fig. 4). Furthermore, V^+V^- chains are seen on occasion in wider rings. We speculate that that these are transient states formed during relaxation from magnetic saturation to the CF state but have been pinned due to defects. If so, it is possible that the formation of V^+V^- pairs is a fundamental part of the said relaxation, at least for certain ring dimensions. In addition, we map remanent configurations as a function of ring thickness and width.

Arrays of Au(2 nm)/$Ni_{80}Fe_{20}$(L=30,40,50,60,70 nm) rings were defined on thermally oxidized Si substrates by electron-beam lithography and lift off. The outer ring diameter was kept constant at 2 μm. Arrays in adjacent rows differed only in ring width w (from 200 to 700 nm in steps of 100 nm). The deposition of the metal layers was carried out in a single growth run at room temperature by electron-beam evaporation under ultrahigh vacuum conditions using a shutter mask at a growth rate of approximately 1 Å/min monitored by a precalibrated quartz microbalance. The base pressure of the system was 4×10^{-10} mbar, while during the growth the pressure was maintained at 1×10^{-9} mbar. Inter-ring spacings were kept at 10 μm in all arrays (Fig. 2). The magnetic microstructure was imaged at remanence by MFM in the tapping-lift mode, detecting the phase shift. The probe

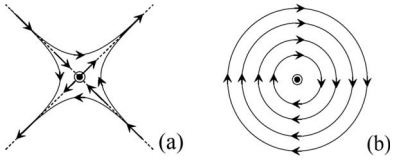

FIG. 1. Schematic diagrams showing (a) V^- and (b) V^+ structure. In the center of each configuration the magnetization tilts out of plane.

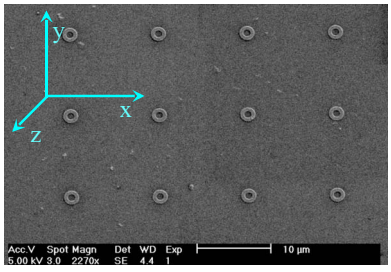

FIG. 2. (Color online) SEM micrograph of a (w,L) =(500 nm, 60 nm) ring array with the coordinate system used in the text marked out.

tips were commercial low-moment tips, magnetized along $+z$. Prior to imaging, all arrays were subjected to a saturating in-plane magnetic field of 5.2 kOe along $+y$. Tip perturbations, i.e., effects on the sample's magnetic structure from the tip's stray field, were systematically monitored by scanning along both $\pm y$ directions and at times by scanning along different angles and lift heights, h_z, varying between 70 and 35 nm. As an aid to interpreting experimental images, we computed MFM contrast maps from micromagnetically obtained magnetization distributions and compared to experiment. The magnetization configurations were calculated using the Object Oriented MicroMagnetic Framework (OOMMF) package.[22] Typical material constants for permalloy were chosen: 800 kA/m, 13 pJ/m, and 0, corresponding to the saturation magnetization, exchange stiffness constant, and magnetocrystalline anisotropy constant, respectively. The discretization cell size was $5\times5\times\Delta z$ nm^3, where Δz is the thickness of the discretization cell along z [in two-dimensional (2D) cases $\Delta z=L$]. All calculations were done at zero temperature. The procedure for obtaining the static magnetization distributions was by arranging spins close to V^+, $2V^+$, and $V^+V^-V^+$ configurations, then using the conjugant-gradient minimization scheme to reach a local energy minimum. From the magnetic configurations, MFM contrasts were obtained by calculating the phase shift measured by the microscope $\Delta\Phi\propto\hat{n}\cdot\vec{\nabla}F_n$, where $\hat{n}$ is collinear with the direction of the MFM cantilever oscillation[23] and $F_n=\hat{n}\cdot\vec{F}$, where $\vec{F}$ is the force on the tip. We employed the point-probe approach,[24] using the dipole contribution.[25,26] For simplicity, we let $\hat{n}=\hat{z}$ (neglecting any tilting of the cantilever[23]), i.e., $\hat{n}\cdot\vec{\nabla}F_n=(\partial/\partial z)F_z$. The MFM tip was approximated by a rigid magnetic point dipole $\vec{m}_t$ with its moment solely along $+z$ ($m_{t,x}=m_{t,y}=0$), located at the (imaginary) distance δ_z with respect to the tip apex along z. Writing $(\partial/\partial z)F_z$ in terms of $(\partial^2/\partial z^2 H_{s,z})$, $\Delta\Phi$ is expressed as (in degrees)[26]

$$\Delta\Phi=-\frac{180Q}{\pi k}\left[\mu_0 m_{t,z}\frac{\partial^2 H_{s,z}}{\partial z^2}\right], \tag{1}$$

where $Q\approx230$ is the measured quality factor of the cantilever, $k=2.8$ N/m is the cantilever spring constant, $m_{t,z}=3\times10^{-17}$ Am^2, and $H_{s,z}$ is the sample's stray field. Since the coating geometry and effective magnetic volume of the tip is unknown, δ_z cannot be calculated theoretically and thus acts as a fitting parameter. However, since we require only a qualitative determination of the MFM contrast, a systematic variation in δ_z was not performed. Furthermore, tip-induced perturbations were not taken into account in the calculations. Finally, the scan heights h_z were considered large enough so that each computational cell in the computed magnetization distribution could be treated as a cell-centered point dipole (i.e., the field at a point on the MFM scanning plane is the superposition of dipole fields from all cells).

From three-dimensional (3D) micromagnetic simulations, we find that the magnetization distributions investigated here are not homogeneous along z, where the magnetization twists around the vortex and antivortex cores [Figs. 4(e)–4(g)]. However, resulting differences in computed MFM contrasts from 3D and 2D representations are negligible [Figs. 4(b) and 4(d)]. Furthermore, specific features, useful to further clarify the experimental magnetic structure, are the bridgelike contrasts appearing between regions separating V^+ and V^- structures. If properly resolved in the experiment, they can be used to directly determine the core polarization, i.e., the direction ($\pm z$) of the out-of-plane component in the center of a V^+ and a V^- (see Fig. 1). This is demonstrated in Fig. 3. The combination of core polarizations in Fig. 3(b) is the one resolved in the experiment since it is the only combination for which the computed bridgelike features [Fig. 3(c)] match the experimental ones [Fig. 3(a)].

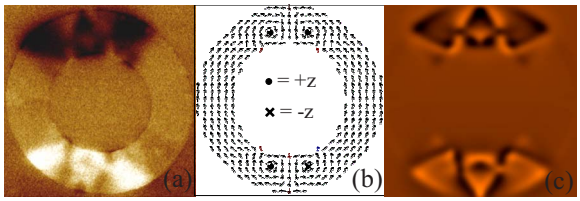

FIG. 3. (Color online) (a) Experimental MFM image of $2V^+$ walls in a $(w,L)=(400\text{ nm},\ 60\text{ nm})$ ring, $h_z=55$ nm. (b) Computed 2D magnetization distribution with core polarizations marked out. (c) Computed MFM contrast of (b), $h_z=55$ nm, $\delta_z=40$ nm.

In the experimental procedure, it is important to note that, for the determination of the stability of the domain walls (i.e., the range of w, L values where the CF state is not the preferred one), the sensitivity to the tip's stray field differs for various ring sizes. First, as w and L increase, the demagnetizing energy will increase until domain walls can no longer be sustained and the CF state is the only one the system will choose.[13] Second, even within the same array, different rings may have different boundary roughness, meaning different domain-wall coercivities. It was observed that some rings were switched into a CF state by the tip and it is even possible that the tip's stray field may switch a ring before it has been imaged. The risk of such cases should increase as w and/or L increases. Thus, it is difficult to determine the domain-wall stability by MFM without performing a systematic study of tip effects, using different tips with various magnetic moments.

We begin by describing the observation of V^- structures in ring elements. Representative configurations were found for $(w,L)=(400\text{ nm},\ 60\text{ nm})$ (Fig. 4). The structure on the top part of the ring in Fig. 4(a) displays contrast indicative of a $V^+V^-V^+$ structure.[14,15] Indeed, setting a configuration in the micromagnetic simulations close to a $V^+V^-V^+$ distribution on the top part (and a $2V^+$ wall at the bottom) and putting the core polarizations appropriately, the resulting local minimum state [Fig. 4(b)] is in excellent agreement with the MFM image [Fig. 4(a)]. Here, the $V^+V^-V^+$ configuration and a $2V^+$ wall coexist in the same ring, which was the case for the majority of observations with $V^+V^-V^+$ structures. Scanning at various angles and lift heights did not alter or erase this structure. We thus verify through this direct observation previous predictions of the occurrence of V^- structures in ring elements.[13] Comparisons made between Figs. 4(c) and 4(d) enable us to assign the correct core polarization to the experimental image. Instances of the pure case with two

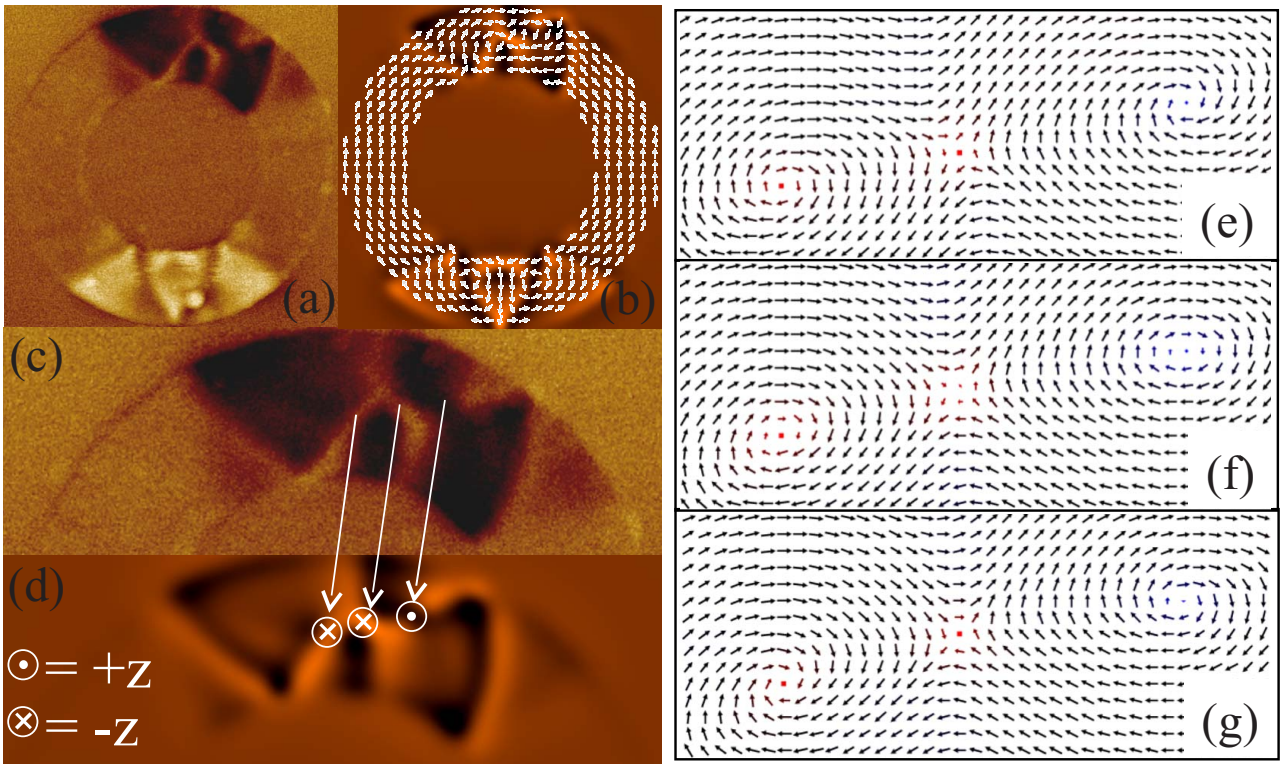

FIG. 4. (Color online) (a) Experimental MFM image of a $(w,L)=(400\ \text{nm},\ 60\ \text{nm})$ ring with a $V^+V^-V^+$ configuration on the top part and a $2V^+$ wall on the bottom part, $h_z=35$ nm. (b) Corresponding 2D magnetization distribution superimposed on the computed MFM contrast (2D) ($h_z=35$ nm, $\delta_z=40$ nm). (c) Blow up of the $V^+V^-V^+$ structure in (a). (d) Computed MFM contrast from 3D calculation ($h_z=35$ nm and $\delta_z=40$ nm) with core polarizations marked out assigned to (c). (e)–(g) The magnetization distribution around the vortex/antivortex cores of the $V^+V^-V^+$ structure on the top, middle, and bottom plane, respectively, of the 3D calculation.

$V^+V^-V^+$ structures were scarce. Either states with two $2V^+$ wall structures (such as in Fig. 3) or the case in Fig. 4 were observed for this ring size. Comparing computed energies between the states in Fig. 3(b) and Fig. 4(b) we find the former to be ~3.6 percent lower in energy, meaning the $2V^+$ wall structures are slightly preferred for this ring size. For $L\leq 50$ nm and $200\leq w\leq 400$ nm, we find predominately V^+ walls in each ring (similar to Ref. 13). A tendency starts toward $2V^+$ wall structures for $L>50$ nm and $200\leq w\leq 500$ nm with the special cases of $V^+V^-V^+$ configurations at $(w,L)=(400\ \text{nm},\ 60\ \text{nm})$. Interestingly, clear cases as in Fig. 4 are only found for rings with $(w,L)=(400\ \text{nm},\ 60\ \text{nm})$. This does not necessarily mean that it is an isolated (w,L) point, but can also mean a narrow (w,L) range for such structures. Therefore, a refinement of (w,L) steps is necessary to resolve this matter. At $(w,L)=(500\ \text{nm},\ 50\ \text{nm})$ we start to see V^+ and $2V^+$ wall structures trapped in the same rings, indicating that we are close to a boundary line in the magnetic phase diagram. This makes the domain walls more sensitive to tip perturbations. However, once formed, the walls do not transform due to tip effects (excluding cases when a ring is pushed into the CF state). For rings of $w\geq 600$ nm it is noticed that the occurrence of CF states increases dramatically to the point of

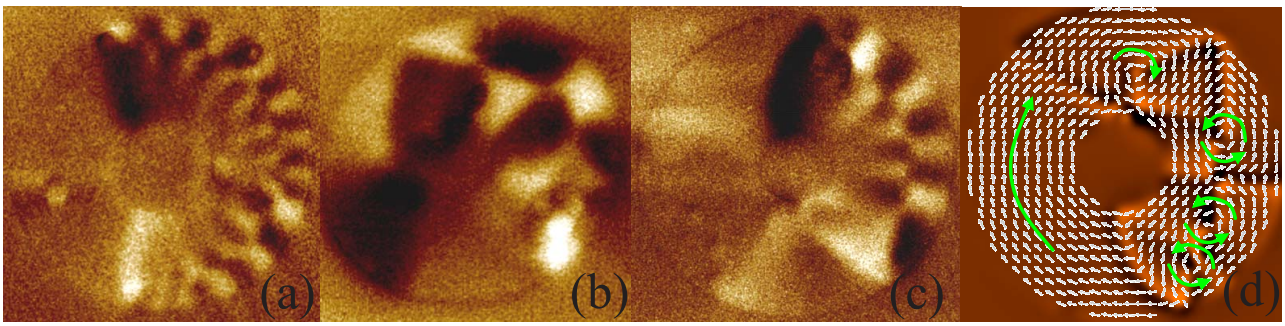

FIG. 5. (Color online) Experimental MFM images of V^+V^- chains in (a) $(w,L)=(600\ \text{nm},\ 50\ \text{nm})$. (b) $(w,L)=(700\ \text{nm},\ 40\ \text{nm})$. (c) $(w,L)=(700\ \text{nm},\ 50\ \text{nm})$. (d) Snapshot of a simulated magnetization configuration in the ring in (c) during relaxation to the CF state with its computed MFM contrast, discretization: $4\times 4\times L\ \text{nm}^3$.

domination and observations of V^+, $2V^+$, and $V^+V^-V^+$ wall structures are rare. This is supported by micromagnetic computations whereby for $w \geq 600$ nm, only three ring dimensions—$(w,L)=(600\ \text{nm}, 30\ \text{nm})$, (600 nm, 40 nm), and (700 nm, 30 nm) having V^+, $2V^+$, and V^+ wall structures, respectively—were sustainable. Experimentally, we do find corresponding occurrences as seen in the simulations for such wide rings, although since they are very easily switched to CF states by the tip (making it difficult to conclude the dominant type of domain wall) we assign to them the CF state with respect to the MFM tip. Moreover, fascinating configurations comprised of V^+V^- chains are found on occasion in $(w=700\ \text{nm}, L=40,50\ \text{nm})$ and $(w=600\ \text{nm}, L=50\ \text{nm})$ rings (Fig. 5), although the majority of them are in the CF state, as also found in the micromagnetic simulations. We simulated the relaxation from saturation to the CF state for a $(w=700\ \text{nm}, L=50\ \text{nm})$ ring [first saturating along $+y$ with 5.2 kOe ($\alpha=0.9$), then relaxing in zero field ($\alpha=0.1$), solving the Landau-Lifshitz equations]. A snapshot during the relaxation is shown in Fig. 5(d). Notice the formation of V^+V^- pairs, similar to Fig. 5(c). Therefore, we propose that these observed configurations are transient states that have been pinned by defects when relaxing from saturation to the CF state. If so, then they are snapshots of part of the relaxation process. Elaborating on this idea, it is then possible that formation and annihilation of V^+V^- pairs plays a fundamental role in the relaxation process, at least for these wide rings. The observed domain-wall types in the onion state as a function of w and L are shown in Fig. 6.

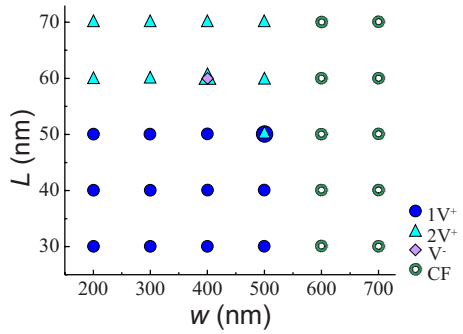

FIG. 6. (Color online) Observed states as a function of (w,L).

In summary, we have experimentally verified the occurrence of the predicted V^- wall structures in single-layer ring elements. Furthermore, observations of V^+V^- chains in wider rings opens the possibility that formation and annihilation of V^+V^- pairs constitute fundamental parts of the relaxation path from the saturated to CF state at least for the ring sizes in Fig. 5. Finally, a phase diagram of different onion-state domain walls as a function of w and L is presented.

The authors acknowledge T. Hayward and C. Ross for fruitful discussions. P.E.R. acknowledges financial support from the Swedish Research Council and J.H.L. from the Department of Physics and Clare College. This work was funded by EPSRC RG 48046.

*per24@cam.ac.uk

[1] J.-G. Zhu, Y. Zheng, and G. A. Prinz, J. Appl. Phys. **87**, 6668 (2000).
[2] M. M. Miller, G. A. Prinz, S.-F. Cheng, and S. Bounnak, Appl. Phys. Lett. **81**, 2211 (2002).
[3] G. A. Prinz, J. Magn. Magn. Mater. **200**, 57 (1999).
[4] S. A. Wolf, D. D. Awschalom, R. A. Buhrman, J. M. Daughton, S. von Molnar, M. L. Roukes, A. Y. Chtchelkanova, and D. M. Treger, Science **294**, 1488 (2001).
[5] D. L. Graham, H. A. Ferreira, and P. P. Freitas, Trends Biotechnol. **22**, 455 (2004).
[6] R. D. McMichael and M. J. Donahue, IEEE Trans. Magn. **33**, 4167 (1997).
[7] Y. Nakatani, A. Thiaville, and J. Miltat, J. Magn. Magn. Mater. **290–291**, 750 (2005).
[8] M. Klaui, C. A. F. Vaz, J. A. C. Bland, L. J. Heyderman, F. Nolting, A. Pavlovska, E. Bauer, S. Cherifi, S. Heun, and A. Locatelli, Appl. Phys. Lett. **85**, 5637 (2004).
[9] M. F. Lai, Z. H. Wei, C. R. Chang, J. C. Wu, J. H. Kuo, and J. Y. Lai, Phys. Rev. B **67**, 104419 (2003).
[10] M. Laufenberg *et al.*, Appl. Phys. Lett. **88**, 052507 (2006).
[11] J. Rothman, M. Klaui, L. Lopez-Diaz, C. A. F. Vaz, A. Bleloch, J. A. C. Bland, Z. Cui, and R. Speaks, Phys. Rev. Lett. **86**, 1098 (2001).
[12] M. Kläui, C. A. F. Vaz, L. Lopez-Diaz, and J. A. C. Bland, J. Phys.: Condens. Matter **15**, R985 (2003).
[13] M. H. Park, Y. K. Hong, B. C. Choi, M. J. Donahue, H. Han, and S. H. Gee, Phys. Rev. B **73**, 094424 (2006).
[14] K. Shigeto, T. Okuno, K. Mibu, T. Shinjo, and T. Ono, Appl. Phys. Lett. **80**, 4190 (2002).
[15] T. Okuno, K. Mibu, and T. Shinjo, J. Appl. Phys. **95**, 3612 (2004).
[16] M. Klaui *et al.*, Appl. Phys. Lett. **88**, 232507 (2006).
[17] K.-S. Lee, S. Choi, and S.-K. Kim, Appl. Phys. Lett. **87**, 192502 (2005).
[18] R. Hertel and C. M. Schneider, Phys. Rev. Lett. **97**, 177202 (2006).
[19] S. Gliga, M. Yan, R. Hertel, and C. M. Schneider, Phys. Rev. B **77**, 060404(R) (2008).
[20] R. Hertel, W. Wulfhekel, and J. Kirschner, Phys. Rev. Lett. **93**, 257202 (2004).
[21] K. Kuepper, M. Buess, J. Raabe, C. Quitmann, and J. Fassbender, Phys. Rev. Lett. **99**, 167202 (2007).
[22] OOMMF is available for free from NIST at http://math.nist.gov/oommf
[23] D. Rugar, H. J. Mamin, P. Guethner, S. E. Lambert, J. E. Stern, I. McFadyen, and T. Yogi, J. Appl. Phys. **68**, 1169 (1990).
[24] U. Hartmann, Phys. Lett. A **137**, 475 (1989).
[25] L. Lohau, S. Kirsch, A. Carl, and E. F. Wassermann, J. Appl. Phys. **86**, 3410 (1999).
[26] L. Lohau, S. Kirsch, A. Carl, and E. F. Wassermann, Appl. Phys. Lett. **76**, 3094 (2000).